Transformation of Delta-Ferrite during the Postweld Heat Treatment of Type 316L Stainless Steel Weld Metal

Transformation kinetics are rationalized on the basis of "normalized equivalent chromium content"

BY T. P. S. GILL, M. VIJAYALAKSHMI, J. B. GNANAMOORTHY AND K. A. PADMANABHAN

ABSTRACT. The microstructural changes in Type 316L stainless steel weld metal aged at 773, 873 and 973 K were studied using an electrochemical extraction method, magnetic measurements, x-ray diffraction and microscopic techniques. At 773 K, slow and partial decomposition of delta-ferrite occurred, resulting predominantly in secondary austenite. In contrast, at 873 and 973 K the delta-ferrite transformed in a short time, mainly into sigma phase. By comparing the present results with values reported in the literature, a "normalized equivalent chromium content" is proposed to rationalize the transformation kinetics of delta-ferrite.

Introduction

Type 316 stainless steel is preferred over Type 304 as a major structural material for the liquid metal fast breeder reactors due to its superior mechanical properties at elevated temperatures. During the operation of the reactor, the alloy in both the wrought and welded conditions is exposed to elevated temperatures (~ 823 K) for long periods. Data on the behavior of wrought 316 stainless steel are more extensive (Refs. 1-4) than those concerning the weld metal.

In order to reduce the crack susceptibility, the chemistry of the weld metal is suitably altered to provide some delta-ferrite (normally between 2 and 10%). However, the presence of delta-ferrite is detrimental under certain conditions: (1) an enhanced attack of the weldments is seen in certain corrosive media (Refs. 5, 6), and (2) embrittlement results from the precipitation of sigma at high temperatures (Refs. 7-13). Though such general trends in the behavior of the weld metal are recognized, very little quantitative information is available on the kinetics of decomposition of delta-ferrite or the growth of secondary phases and their effect on the mechanical properties of the weld metal.

The present paper describes the results of an investigation to understand the microstructural changes that take place in Type 316L stainless steel weld deposits as a function of temperature and time. An important feature was the use of an electrochemical technique for the extraction and quantitative estimation of the secondary phases present in the weld metal.

Experimental Procedure

Material and Heat Treatment

Using the gas tungsten arc (GTA) welding process, bead-on-plate weld pads were prepared by depositing 316L stainless steel filler metal on a 25 mm (1 in.) thick mild steel base plate dimensioned 300 × 100 mm (12 × 4 in). The deposit was built up to a size of 300 × 25 × 25 mm (12 × 1 × 1 in.). The welding direction and bead sequence were kept the same for all the pads. The stainless steel deposit was sectioned at a distance of approximately 10 mm (0.4 in.) from the mild steel base, to avoid the deposit which might have been contaminated by dilution from the base metal. The chemical composition of the weld deposit and the welding variables employed are given in Tables 1 and 2, respectively. Specimens of 20 × 10 × 3 mm (0.8 × 0.4 × 0.12 in.) were machined from the weld pad in a plane parallel to the welding direction and were encapsulated in quartz tubes under an argon atmosphere. The capsules were then aged at 773, 873 and 973 K for different durations, ranging from 0.2 to 5000 h.

Delta-Ferrite Measurement

The delta-ferrite contents of the as-deposited and aged specimens were determined using a Magne-Gage, which was calibrated by a No. 3 magnet in accordance with the procedures described in AWS A4.2-74 (Ref. 14). During the course of the investigations, the Magne-Gage was calibrated from time to time, but no significant change in the calibration curve was noticed. A large number of readings (about 40) were taken on each specimen to arrive at the average value of the ferrite number (FN).

Identification of Secondary Phases

The secondary phases present in the as-deposited and aged specimens were extracted by selective electrochemical dissolution of the austenite matrix. The dissolution process was carried out in a

BY T. P. S. GILL, M. VIJAYALAKSHMI and J. B. GNANAMOORTHY are with the Materials Development Laboratory, Indira Gandhi Center for Atomic Research, Kalpakkam, Tamil Nadu, India. K. A. PADMANABHAN is with the Department of Metallurgical Engineering, Indian Institute of Technology, Madras, India. He is presently on leave as an Alexander Von Humboldt Fellow at a university in the Federal Republic of Germany.

Table 1—Chemical Composition of the Weld Deposit (wt-%)

C	Mn	Si	Cr	Ni	Mo	N	S	P
0.015	1.75	0.31	19.10	13.80	2.59	0.021	0.004	0.02

standard polarization cell containing a deaerated electrolyte of composition 3.6 N sulphuric acid and 0.1 N ammonium thiocyanate. The dissolution potential of −80 mV was maintained constant potentiostatically with reference to a saturated calomel electrode. The details of the extraction procedure have been reported elsewhere (Refs. 15,16).

The residue obtained by the bulk extraction process was dried and weighed to determine the total weight percent of the secondary phases in the matrix. The identification of the precipitates was carried out using a Philips PM 8203 x-ray diffractometer fitted with a graphite monochromator. Diffraction profiles were recorded using a copper target at 30 kV.

Microstructural Studies

Microstructural changes in the weld metals were characterized employing both optical and electron microscopic techniques. The samples for optical microscopy were mechanically polished and chemically etched to reveal the microstructures. The as-deposited sample was etched with the Murakami etchant, while the thermally aged specimens were etched in a modified Murakami etchant (30 g KOH, 30 g K_3 [Fe $(CN)_6$] and 150 ml H_2O). Samples for transmission electron microscopy were polished at 40 V in a solution of 5% perchloric acid and 95% acetic acid, maintained at 15°C (59°F). The thin foils were observed using a Philips EM 400 transmission electron microscope operating at 120 kV.

Results and Discussion

The results of the present study, obtained from the various techniques, are classified into (1) dissolution of delta-ferrite and (2) evolution of secondary phases.

Dissolution of Delta-Ferrite

The ferrite content of the as-deposited weld metal was estimated by magnetic (using the Magne-Gage) and electrochemical dissolution techniques. The values obtained agreed very well, *i.e.*, 7.1 FN (range: 5.6 to 9.4 FN) and 6.2 wt-%, respectively. The ferrite content values were measured before and after aging at various temperatures. These were converted to fraction of ferrite transformed and plotted as a function of the aging time—Fig. 1. It is clear that the transformation of delta-ferrite was sluggish at 773 K—only about half of the initial ferrite had transformed despite aging for 5000 h. However, the transformation rate became appreciably faster at 873 and 973 K. At 873 K, all the ferrite was dissolved in slightly over 20 h, whereas at 973 K, only 2 h of aging was sufficient to transform the ferrite completely. This observation can be explained on the basis of the existence of a C-curve behavior for the dissolution of delta-ferrite in Type 316 stainless steel, with the maximum rate of transformation being present at ~1123 K (Ref. 7). (Another important feature which influences the dissolution of delta-ferrite is the kinetics of precipitation of the secondary phases, which is discussed later.)

Microscopic studies were carried out to identify the nature of the delta to gamma transformation. Figures 2A and 2B show the optical and transmission electron micrographs, respectively, of a transverse section of an as-welded sample, revealing a well-interconnected, vermicular morphology of delta-ferrite. The structure can be classified into two distinct regions, namely (1) the primary dendrite core (marked A) and (2) the secondary dendrite arm (marked B). Figures 2C and 2D show optical microstructures of the weld metal after aging at 773 K for 5000 h. In Fig. 2D, the preferential etching of the magnetic delta-ferrite particles (magnet "on" position) delineates them from the transformed delta-ferrite. It was seen that the "secondary dendrite arms" of the delta-ferrite transformed faster than the "primary dedrite cores." This could be attributed to the shorter diffusion distances and possible differences in their chemical compositions. The "primary dendrite core" was found to transform into austenite by an epitaxial growth of gamma in delta-ferrite, as shown in Figs. 3A–3C. The present evidence for the epitaxial growth of austenite inside ferrite in a duplex weld metal is in contrast to the cooperative mechanism of the growth of carbide and austenite observed earlier (Ref. 17).

Table 2—Welding Variables

Welding process	Gas tungsten arc (manual)
Welding wire	AISI 316L stainless steel
Shielding gas	Argon
Welding wire diameter	2.5 mm
Polarity	DC electrode negative
Welding current	110 A
Welding speed[a]	6 cm min^{-1}
Welding wire feed rate[a]	9.1 cm min^{-1}
Argon flow rate	4.5 s/l min^{-1}

[a]Since GTA welding was carried out manually, the welding wire feed rate and the welding speed are approximate and represent average values.

Evolution of Secondary Phases

A number of secondary phases, like carbides, chi (χ) and sigma (σ), evolve during the postweld heat treatments of duplex weld metals. Their morphologies, sites of nucleation and growth kinetics are described in this section.

As-Welded Metal

It was seen earlier that the as-welded samples have a well interconnected structure of delta-ferrite. Transmission electron microscopic studies revealed the austenite/ferrite interface to be devoid of any precipitation of carbides, which suggests a high cooling rate. The absence of any precipitation in the as-welded specimen was also corroborated by an x-ray diffractogram (Fig. 4), obtained from the residue collected after the electrochemical dissolution of austenite. The observation is in contrast to those pertaining to high heat input weld metal (Ref. 18), where the precipitation of carbides along the interfaces has been reported for the as-welded condition.

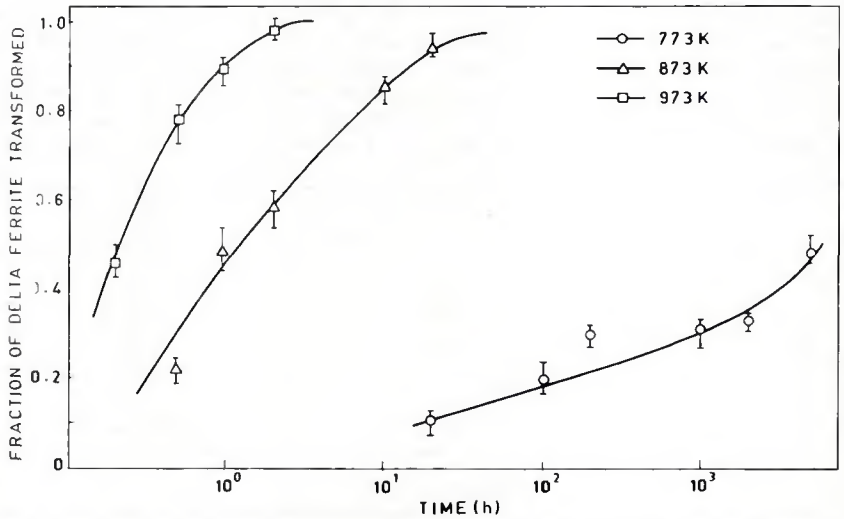

Fig. 1—Fraction of delta-ferrite transformed on aging at 773, 873 and 973 K, as a function of aging time

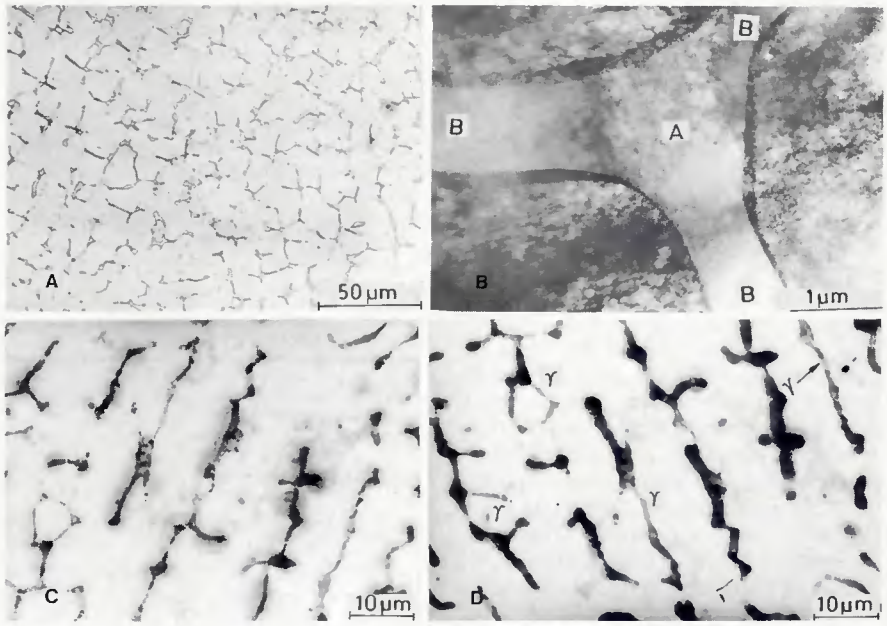

Fig. 2 — A — Optical and B — transmission electron micrographs of the transverse section of as-welded samples. Figure 2B shows the "primary dendrite core" (A) and the "secondary dendrite arms" (B). C and D — Optical micrographs of samples aged at 773 K for 5000 h. After the modified Murakami etching, the sample was magnetically etched to reveal the preferential transformation of the secondary dendrite arms into austenite. Figure 2C is with the magnet in the "off" position and Fig. 2D is with the magnet on

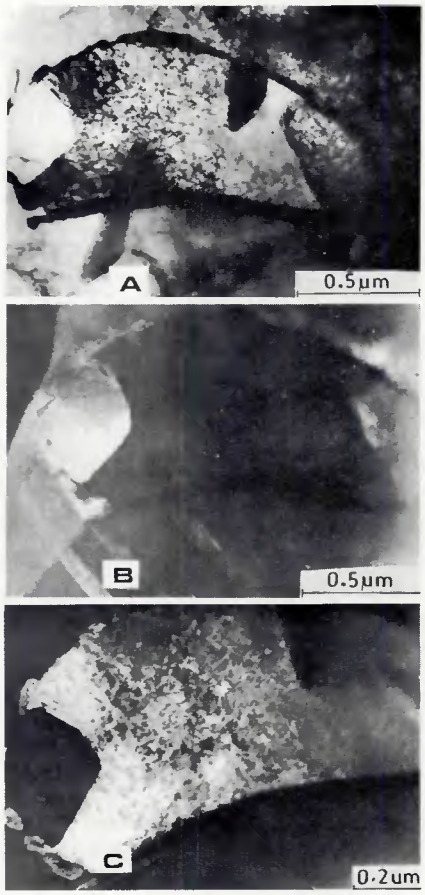

Fig. 3 — Transmission electron micrographs of sample aged at 773 K for 5000 h showing the growth mechanism of austenite into a massive delta-ferrite core. A — Bright field image; B and C — Dark field images with austenite and delta-ferrite reflections, respectively

Aging at 773 K

Optical microscopic studies of the samples aged at 773 K revealed a structure essentially similar to that of the as-welded samples, but with two differences: (1) a lesser degree of interconnectivity of ferrite, implying a delta to gamma transformation, and (2) appearance of secondary phases, mostly within the delta-ferrite. A typical micrograph, illustrating the above features in a sample aged for 5000 h, is shown in Fig. 5A. A magnified view of a delta-ferrite particle containing the secondary phases is shown in the transmission electron micrograph — Fig. 5B. In addition to extensive precipitation inside the ferrite particle, an almost continuous film of a secondary phase was found to decorate some of the austenite/ferrite interfaces. No dark field image could be obtained due to the thickness of the film. This film is probably $M_{23}C_6$, since its morphology is similar to that of $M_{23}C_6$ reported in previous studies (Ref. 19).

It is seen that the carbides in the weld metal prefer the high energy delta/gamma interfaces, as compared to the high angle grain boundaries present in the wrought alloy. The other secondary phases (sigma, chi, etc.) grow within the delta-ferrite for the following reasons: (1) availability of more chromium and molybdenum and (2) higher diffusion rates in ferrite than in austenite. These factors ultimately lead to the faster growth rates of the secondary phases in the duplex weld metal. The localized nature of the precipitation reactions within delta-ferrite implies that the growth kinetics of the secondary phases could be similar to that of ferritic, rather than austenitic, stainless steel — at least as long as delta-ferrite is present.

A quantitative estimation of the weight fraction of the precipitates is listed in Table 3. It is seen that at 773 K precipitation was sluggish, with only 1.67% of the total weight being extracted as precipitates, even after aging for 5000 h. It may be pointed out here that these values are likely to be underestimated due to the electrochemical dissolution of some portion of the untransformed delta-ferrite. Earlier investigators have reported (Refs. 10, 20) that the chemical composition of the delta-ferrite particles in the aged samples, and in particular those with interfaces lined with a carbide film, is very near the chemical composition of austenite. Therefore, it is possible that the "depleted" delta-ferrite particles dissolve along with the austenite during the electrochemical extraction process in which only the secondary phases enriched in chromium relative to the matrix can be extracted.

The identification of the precipitates extracted after 5000 h of aging at 773 K is shown in Fig. 5C. The x-ray diffractogram reveals the presence of delta-ferrite, carbide, chi and sigma. These phases were found to be present at all aging times, as

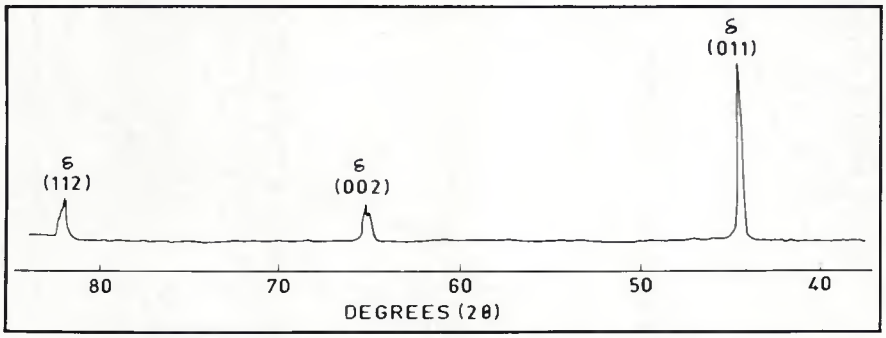

Fig. 4 — X-ray diffractogram of the residue extracted by an electrochemical technique from the as-deposited weld metal

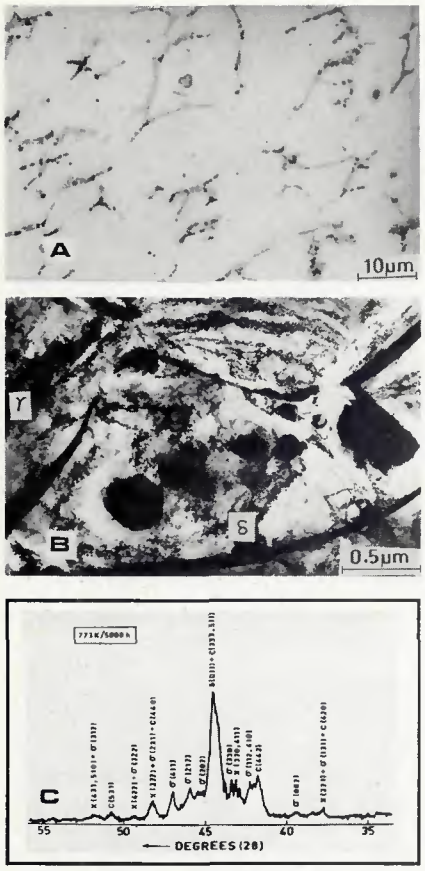

Fig. 5—A—Optical micrograph of sample aged at 773 K for 5000 h which suggests the presence of secondary phases within delta-ferrite. B—Electron micrograph of sample aged at 773 K for 5000 h confirms the presence of secondary phases within delta-ferrite. Also obvious is the presence of an almost continuous film of carbide at the austenite/ferrite interface. C—Identification of the secondary phases in the residue extracted from a sample aged at 773 K for 5000 h by x-ray diffraction

Table 3—Total Amount of Precipitate Extracted, Fraction of Delta-Ferrite Transformed and Results of X-ray Diffraction Analyses

Aging Temperature (K)	Aging Time (h)	Total Amount of Precipitate (wt-%)	Fraction of Delta-Ferrite Transformed	Phases Present
As-deposited	–	6.2	0.00	δ
	200	0.83	0.29	δ, σ, χ, $M_{23}C_6$
773	2000	0.87	0.35	δ, σ, χ, $M_{23}C_6$
	5000	1.67	0.48	δ, σ, χ, $M_{23}C_6$
	2	1.46	0.58	σ, $M_{23}C_6$
	20	4.30	0.93	σ, χ, $M_{23}C_6$
873	200	5.80	1.00	σ, $M_{23}C_6$
	2000	6.31	1.00	σ, $M_{23}C_6$
	5000	8.96	1.00	σ, $M_{23}C_6$
	0.5	4.22	0.78	σ, $M_{23}C_6$
	2	5.19	0.98	σ, $M_{23}C_6$
	20	8.04	1.00	σ, $M_{23}C_6$
973	200	8.63	1.00	σ, $M_{23}C_6$
	2000	12.45	1.00	σ, $M_{23}C_6$
	5000	13.40	1.00	σ, $M_{23}C_6$

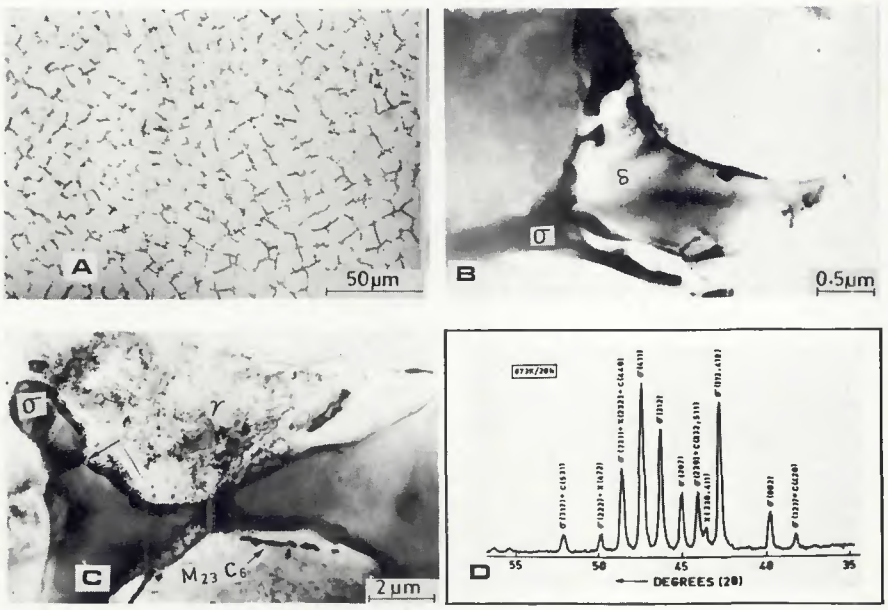

Fig. 6—A—Optical micrograph of weld metal aged at 873 K for 20 h and etched specifically for sigma and carbide. B—Nucleation of sigma along the dendrite arms of delta-ferrite in a sample aged at 873 K for 2 h. C—Impingement of independently nucleated and grown sigma particles, leading to grain boundaries (marked by arrows) within sigma in a sample aged at 873 K for 200 h. D—X-ray diffractogram of residue extracted from weld metal aged for 20 h, showing a small amount of chi

indicated in Table 3. The relative quantity of each phase is difficult to estimate, in view of the low total precipitate content.

Aging at 873 K

Precipitation at 873 K was quite different from 773 K, and the kinetics were considerably faster. The principal product during the transformation of delta-ferrite at this temperature was sigma—Fig. 6A. The morphology of sigma was similar to that of delta-ferrite, at least initially. This suggests that the nucleation and growth of sigma is perhaps confined to the ferrite regions. Further confirmation was obtained by electron microscopic studies. Figure 6B is a transmission electron micrograph of a specimen aged for 2 h, showing the preferential nucleation and growth of the sigma phase along the secondary dendrite arms of delta-ferrite. On further aging, these particles grew independently, and the replacement of ferrite by sigma occurred when two or more sigma particles grew contiguously. Distinct grain boundaries between two such sigma particles could be observed, as shown in Fig. 6C, for a sample aged up to 200 h. It is clear from the micrograph that during the transformation of delta-ferrite to sigma and austenite, the original austenite/ferrite interface migrates into the delta-ferrite and advances ahead of the carbides, leaving them as isolated particles in the austenite.

The weight percentages of the secondary phases are given in Table 3. A larger amount of total precipitates is obtained after 5000 h of aging, *i.e.*, 8.96 wt-%, in contrast to the 1.67 wt-% obtained at 773 K. For all aging conditions except 20 h (Table 3), these precipitates were identified by x-ray diffraction as a mixture of sigma and carbide. In specimens aged for 20 h, however, a small amount of chi was also observed in the x-ray pattern—Fig 6D. It appears that the

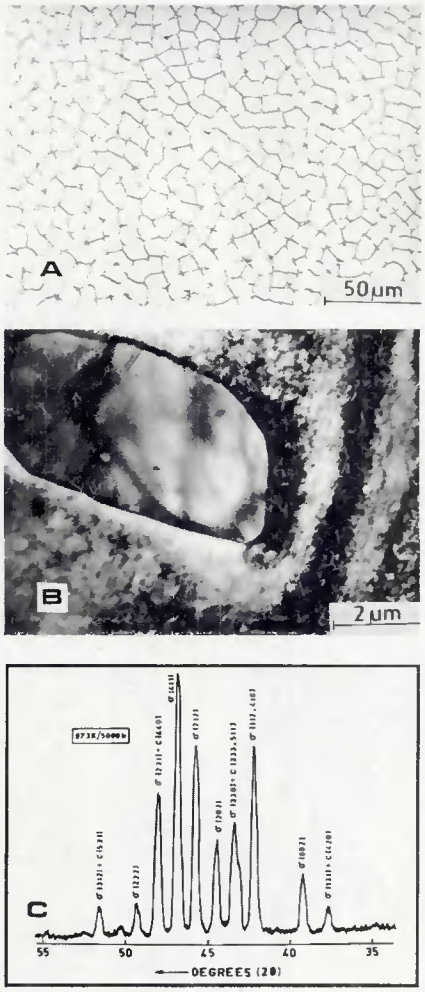

Fig. 7 — A — Optical micrograph of weld metal aged at 973 K for 2 h, showing the complete transformation of delta-ferrite to sigma. B — Electron micrograph of an isolated sigma phase particle after 5000 h at 973 K. C — X-ray diffractogram of residue extracted from weld metal aged at 973 K for 5000 h

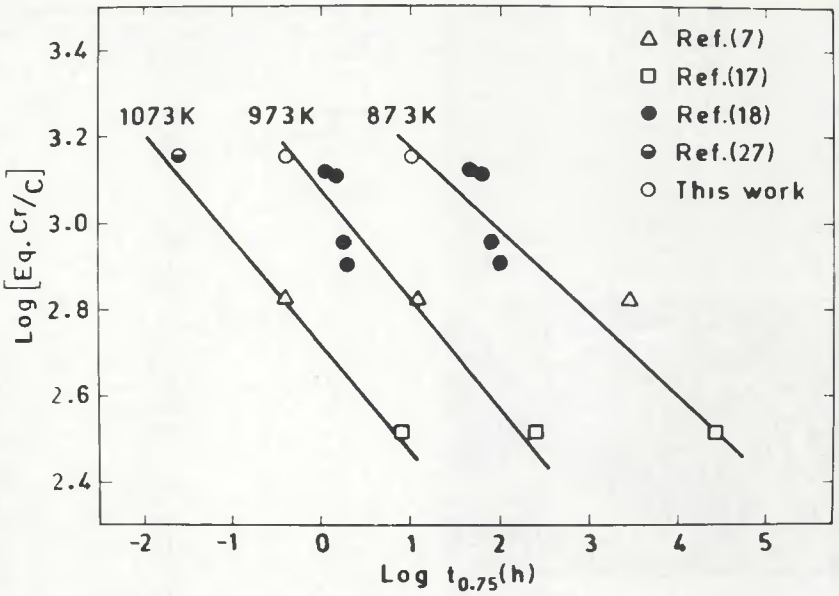

Fig. 8 — The variation of log (normalized equivalent chromium content) with time of aging required to transform 0.75 fraction of the initial ferrite content ($t_{0.75}$) at 873, 973 and 1073 K

formation of chi is favored less at 873 K than at 773 K. It could be due to the enhanced, preferential growth of sigma at higher temperatures, which in turn is facilitated by the low level of carbon in the present alloy.

Aging at 973 K

The aging process at 973 K was similar to 873 K, except for an increase in the growth rate of the secondary phases. The growth of the sigma phase was the fastest at 973 K, and within 2 h sigma was present as a continuous network — Fig. 7A. Further aging leads only to the spheroidization of sigma (discussed later), leaving individual particles in austenite — Fig. 7B. The higher growth rate of the precipitation process is clear from Table 3. It is seen that 4.2 wt-% is obtained as precipitates within 0.5 h of aging, and the amount of precipitates after 5000 h was at a maximum at 973 K (13.4 wt-%) (as compared to the other two temperatures discussed previously). These precipitates were identified as sigma and carbide — Fig. 7C. The complete absence of the chi phase at all aging times is indicated in Table 3.

Tavassoli, *et al.* (Ref. 21), have reported the presence of a needle-like Laves phase, *i.e.*, Fe_2Mo precipitates and $M_{23}C_6$ carbides in austenite, on aging weld metals at 923 K for 38,000 h. However, in the present experiments no precipitation within austenite could be observed, possibly because of the shorter aging times employed.

Influence of Precipitation on the Dissolution of Delta-Ferrite

The microstructural instability of the austenitic stainless steel weld metal can be rationalized on the basis of the relative stability of delta-ferrite with respect to that of austenite and sigma (Refs. 22, 23). The two cases of stainless steel weld deposits with low and high carbon contents are discussed below.

When the carbon content is high, the ferrite becomes depleted in chromium and molybdenum due to the rapid precipitation of carbide at the austenite/ferrite interface, and so the ferrite composition approaches that of austenite (Refs. 10, 20). Such ferrite particles either remain as ferrite or transform to austenite on further aging.

On the other hand, when the carbon content is low, as in the present study, the carbide precipitation at the austenite/ferrite interface is sluggish, and the ferrite particles are not depleted of solute elements like chromium and molybdenum. The chemical composition of such particles is very close to that of sigma, and only a simple crystallographic change is required for the transformation of delta-ferrite to sigma (Ref. 20). The ease with which the latter case is encountered is amply demonstrated by the complete replacement of ferrite by sigma within 2 h at 973 K. The nucleation and growth of the sigma phase seems to be the controlling mechanism that determines the rate of ferrite transformation at relatively high temperatures of aging (873 and 973 K). In the literature, the data pertaining to the kinetics of ferrite transformation is a subject of considerable controversy. This is not altogether surprising, as the transformation kinetics of delta-ferrite depend not only on the alloy composition (Refs. 20, 24), but also to some extent on the welding parameters (Ref. 18) which affect the thermal history of the weld metal.

Effect of Alloy Composition

Since carbon level and growth kinetics of sigma influence the transformation kinetics of delta-ferrite significantly, it is essential to characterize the "sigma forming tendency" of the weld metal. Investigations to identify such a parameter have been very successful in the case of wrought stainless steels. Hull (Ref. 25) investigated the effect of chemical composition on the embrittlement of a number of alloys and found a qualitative relationship between brittleness and the amounts of sigma and chi phases present in the alloy. He defined an equivalent chromium content as:

$$\text{Equivalent chromium} = Cr + 0.31Mn + 1.76Mo + 0.97W + 2.02V + 1.58Si + 2.44Ti + 1.70Nb + 1.22Ta - 0.266Ni - 0.177Co$$

A high value of "equivalent chromi-

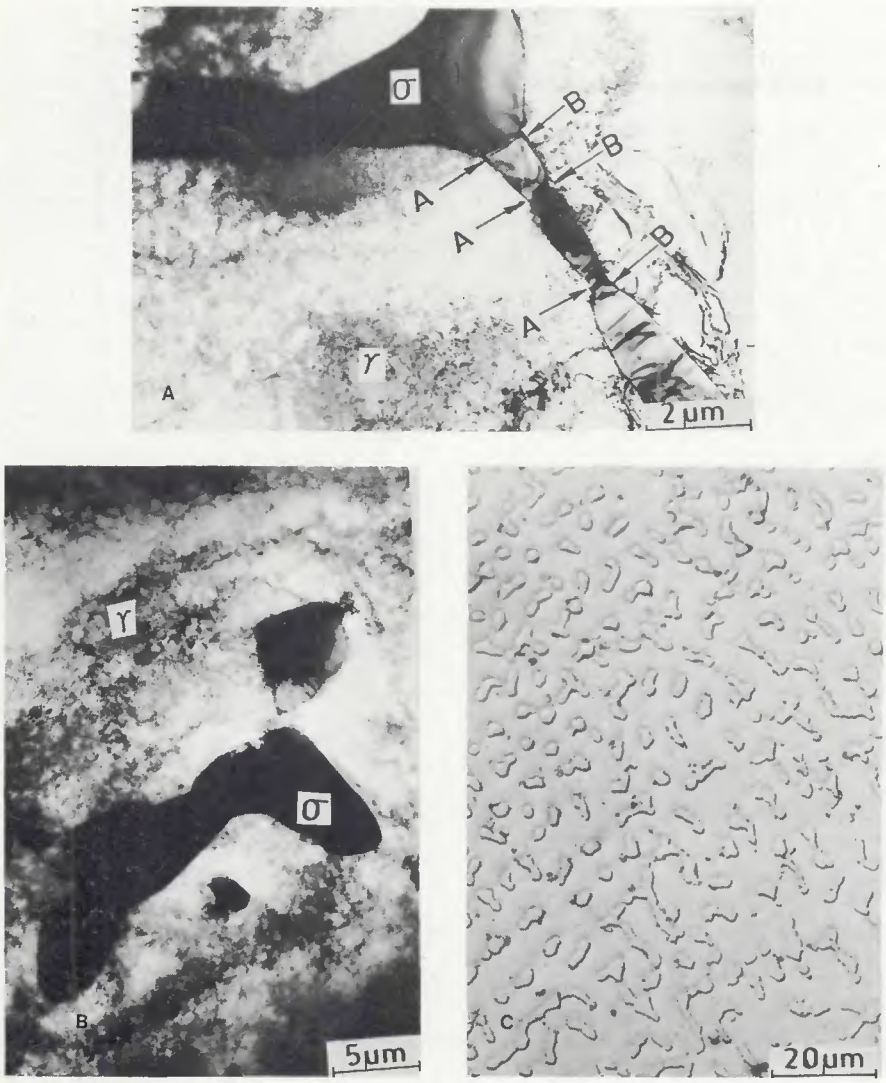

Fig. 9 — A — The onset of shape instability at A and B along sigma/austenite interface, after aging at 873 K for 5000 h. B — The detachment of individual sigma particles from the main dendrites, after the migration of points A and B (Fig. 9A) towards each other. C — Optical micrograph showing the equilibrium morphology of sigma particles after 5000 h at 873 K

um" indicates a strong tendency on the part of the alloy to form sigma. Hull's equivalent chromium does not take into account the contribution of interstitial elements, as in his experiments the presence of carbon and nitrogen did not significantly contribute to the embrittlement of the alloys. However, Grott and Spruiell (Ref. 4) modified Hull's proposal and introduced a concept called "effective equivalent chromium content." The effective equivalent chromium content is essentially Hull's equivalent chromium content remaining in the matrix after the precipitation of carbides. It is found that higher carbon contents in the wrought alloy result in more $M_{23}C_6$ precipitates and decrease the equivalent chromium content of the matrix (which in turn suppresses the formation of intermetallic compounds). Extending the above arguments to the case of weld metals, the choice of equivalent chromium content to characterize the "sigma forming tendency" is found to be reasonable. However, the strong influence of carbon content of the welds has to be incorporated suitably.

Therefore, the equivalent chromium content has been normalized with respect to the carbon content. The present results are compared with those obtained in earlier works (Fig. 8), where the "normalized equivalent chromium contents" are plotted against the time required to transform 0.75 fraction of the initial ferrite content at 873, 973 and 1073 K. It is seen that delta-ferrite transforms at a faster rate in alloys with a higher normalized equivalent chromium content, compared to those having a lower value. This relationship is also found to hold good for other values of the fraction of ferrite transformed (Ref. 27).

Shape Instabilities of Sigma Phase

The rapid transformation of delta-ferrite to sigma in alloys of high normalized equivalent chromium contents leads to a sigma morphology which is essentially similar to that of delta-ferrite. This morphology of sigma is unstable, and therefore "ovulation processes" set in. These processes consist of shape perturbations, consequent "pinching off" of the dendrites, and spheroidization. The presence of such shape instabilities is shown in Fig. 9A, where grooving of the sigma/austenite interface is seen at regular intervals. The progress of such instabilities results in the "drop detachment" process, when the points A and B shown in Fig. 9A meet each other. As a result, a portion of the sigma particle is isolated from the main dendritic sigma, as shown in Fig. 9B. This process is repeated, and an almost equilibrium morphology of sigma is obtained eventually — Fig. 9C. It is seen that most of the sigma particles are isolated and have a spherical shape.

The difference in the surface energy levels of dendritic and spheroidized sigma acts as the driving force for the spheroidization process. The effect of sigma morphology on the mechanical properties of the austenitic stainless steel weld metal has been reported elsewhere (Ref. 26). It is likely that the embrittlement of stainless steel weld metal due to the presence of spheroidized sigma is noticeably less than that due to the presence of dendritic sigma. Further work to determine the kinetics of spheroidization of sigma in Type 316L stainless steel weld metal and its effect on the mechanical properties is in progress.

Conclusions

The decomposition of delta-ferrite is the fastest at 973 K. The explanation for this is based on (1) a C-curve behavior for dissolution and (2) the influence of precipitation of secondary phases.

The secondary dendrite arms with shorter diffusion distances and probably a composition different from that of primary dendrite cores were more susceptible sites for transformation into austenite.

Aging at 773, 873 and 973 K leads to the precipitation of secondary phases like $M_{23}C_6$, chi and sigma. Their morphology and growth kinetics have been documented.

The transformation kinetics of delta-ferrite has been rationalized based on the "normalized equivalent chromium content" of the present alloy.

Acknowledgments

The authors are grateful to Dr. P. Rodriguez, Metallurgy Program Head,

Reactor Research Centre, for his keen interest in the above investigations. They also express their appreciation to Shri P. Kuppuswami for his technical assistance.

References

1. Weiss, B., and Stickler, R. 1972. Phase instabilities during high temperature exposure of 316 austenitic stainless steel. *Metallurgical Transactions* 3:851-866.

2. Lai, J. K. L. 1983. A study of precipitation in AISI Type 316 stainless steel. *Materials Science and Engineering* 58:195-209.

3. Spruiell, J. E., Scott, J. A., Ary, C. S., and Hardin, R. L. 1973. Microstructural stability of thermal-mechanically pretreated Type 316 austenitic stainless steel. *Metallurgical Transactions* 4:1533-1544.

4. Grot, A. S., and Spruiell, J. E. 1975. Microstructural stability of titanium-modified Type 316 and Type 321 stainless steel. *Metallurgical Transactions* 6A, pp. 2023-2030.

5. Gooch, T. G. 1974. A question of ferrite. *The Welding Institute Research Bulletin* 15: 183-188.

6. Garner, A. 1983. Pitting corrosion of high alloy stainless steel weldments in oxidizing environments. *Welding Journal* 62(1):27-34.

7. Thomas, R. G., and Yapp, D. 1978. The effect of heat treatments on Type 316 stainless steel weld metal. *Welding Journal* 57(12):361-s to 366-s.

8. Lai, J. K., and Haigh, J. R. 1979. Delta ferrite transformations in a Type 316 weld metal. *Welding Journal* 58:(1)1-s to 6-s.

9. Thomas, R. G., Nicholson, R. D., and Farrar, R. A. 1984. Creep-rupture properties and microstructure of AISI Type 316L submerged-arc weld metals. *Metallurgical Transactions* 11:61-65.

10. Leitnaker, J. M. 1982. Prevention of chi and sigma phases formation in aged 16-8-2 weld metal. *Welding Journal* 61(1):9-s to 12-s.

11. Lena, A. J. 1954. Effect of sigma phase on properties of alloys. *Metal Progress* 66:94-99.

12. King, R. T., Canonico, D. A., and Brinkman, C. R. 1975. Elevated temperature weldment behavior as related to nuclear design criteria. *Welding Journal* 54(8):265-s to 275-s.

13. Brinkman, C. R., Sikka, V. K., and King, R. T. 1977. Mechanical properties of liquid-metal fast breeder reactor primary piping materials. *Nuclear Technology* 33:76-95.

14. *Standard Procedures for Calibrating Magnetic Instruments to Measure the Delta-Ferrite Content of Austenitic Stainless Steel Weld Metal.* 1974. AWS A4.2-74, American Welding Society, Miami, Fla.

15. Gill, T. P. S., Dayal, R. K., and Gnanamoorthy, J. B. 1979. Estimation of delta-ferrite in austenitic stainless steel weldments by an electrochemical technique. *Welding Journal* 59(12):375-s to 378-s.

16. Gill, T. P. S., and Gnanamoorthy, J. B. 1982. A method for quantitative analysis of delta-ferrite, sigma and $M_{23}C_6$ carbide phases in heat treated Type 316 stainless steel weldments. *J. Mat. Sci.* 17:1513-1518.

17. Thomas, R. G., and Keown, S. R. 1982. *Stress Relief of Austenitic Weldments: Microstructural and Mechanical Property Effects, Mechanical Behaviour and Nuclear Applications of Stainless Steel at Elevated Temperatures.* London, England, The Metals Society, pp. 30-38.

18. Gill, T. P. S., Verma, D. D. N., Seetharaman, V., and Gnanamoorthy, J. B. Decomposition kinetics of delta-ferrite in Type 316 stainless steel welds. The Transactions of the Indian Institute of Metals. Presently unpublished.

19. Vitek, J. M., and David, S. A. 1984. The solidification and aging behavior of Types 308 and 308CRE stainless steel welds. *Welding Journal* 63(8):246-s to 253-s.

20. Slattery, G. F., Keown, S. R., and Lambert, M. E. 1983. Influence of delta-ferrite content on transformation to intermetallic phases in heat-treated Type 316 austenitic stainless steel weld metal. *Met. Tech.* 10:373-385.

21. Tavassoli, A. A., Bisson, A., and Soulat, P. 1984. Ferrite decomposition in austenitic stainless steel weld metals. *Met. Sci.* 18:345-350.

22. LeMay, I., and White, W. E. 1972. Precipitation in austenitic stainless steels. *Metallography* 5:566-569.

23. Raghunathan, V. S., Seetharaman, V., Venkadesan, S., and Rodriguez, P. 1979. The influence of post-weld heat treatments on the structure, composition and the amount of ferrite in Type 316 stainless steel welds. *Metallurgical Transactions* 10A, pp. 1683-1689.

24. Keown, S. R., and Thomas, R. G. 1981. Role of delta-ferrite in thermal aging of Type 316 weld metals. *Met. Sci.* 15:386-392.

25. Hull, F. C. 1973. Effects of composition on embrittlement of austenitic stainless steel. *Welding Journal* 52(3):104-s to 113-s.

26. Gill, T. P. S., Rodriguez, P., Gnanamoorthy, J. B., and Padmanabhan, K. A. 1984. Effect of post-weld aging on the tensile properties of austenitic stainless steel. *Proc. National Welding Seminar,* held at Tiruchirapalli, India, pp. 401-433.

27. Gill, T. P. S., Vijayalakshmi, M., and Gnanamoorthy, J. B. Unpublished work.

28. Gill, T. P. S., and Gnanamoorthy, J. B. Unpublished work.

WRC Bulletin 311
January 1986

Assessment of the Significance of Weld Discontinuities: Effects of Microstructure and Discontinuities upon Fracture Morphology
By C. D. Lundin and C. R. Patriarca

The purpose of this report was to systematically investigate the metallurgical influence of weld metal microstructure, hydrogen presence and loading rate on fracture morphology in the presence of different types of discontinuities. In order to assess the metallurgical significance of weld discontinuities on fracture characteristics, mechanical and nondestructive testing, metallographic and fractographic examination, and hydrogen determinations were used to evaluate E7018, E9018 and E11018 weld metals.

Publication of this report was sponsored by the Subcommittee on Significance of Weld Discontinuities of the Pressure Vessel Research Committee of the Welding Research Council. The price of WRC Bulletin 311 is $14.00 per copy, plus $5.00 for postage and handling. Orders should be sent with payment to the Welding Research Council, Ste. 1301, 345 E. 47th St., New York, NY 10017.